The L3 electromagnetic calorimeter

Yannis Karyotakis

CERN *CH-1211Geneva 23*

ABSTRACT

The L3 electromagnetic calorimeter consists of 10734 BGO crystals. This report gives an overall view of this detector. After summarizing the principles of construction, I will extensively discuss calibration issues, and the performance observed at LEP during its first five years of running.

1 Introduction

L3 [1] is one of the four detectors running on the LEP e^+e^- ring. This detector conceptually differs from a standard e^+e^- collider detector by its emphasis on high resolution measurements of leptons, photons and jets. This is implemented in the experimental setup by a high-resolution muon spectrometer, a precision electromagnetic calorimeter as well as fine-grain hadron calorimetry. High resolution makes the recognition of exclusive final states straightforward. It is essential in detecting rare new phenomena with sufficient signal-to-noise ratio, identifying exclusive and inclusive final states and rejecting backgrounds, analyzing final state properties by measuring particle energy, momentum and reconstructing mass spectra.

The electromagnetic calorimeter consists of 10734 crystals of BGO, $Bi_4Ge_3O_{12}$ shared between two half barrels and two end caps. A three jet event is shown on Figure 1. Even in such a loaded environment, many calorimetric hits and overlapping particles, the detector performs very well. After having identified photons within a hadronic event figure 2 shows the invariant mass of 6 photons from 3 π^0 decays. We clearly observe the η decay to π^0s. L3 is the first LEP experiment to observe χ_c, via the reaction : $e^+e^- \rightarrow Z \rightarrow \chi_{c1} + X, \chi_{c1} \rightarrow J/\Psi\gamma, J/\Psi \rightarrow l^+l^-$. Combining high resolution of the muon spectrometer and the electromagnetic calorimeter we get for the resulting mass difference ($\Delta M = M_{(J/\Psi)\gamma} - M_{J/\Psi}$) the distribution of figure 3, establishing clearly the signal. These two physics [2] examples show the discovery potential of the L3 detector.

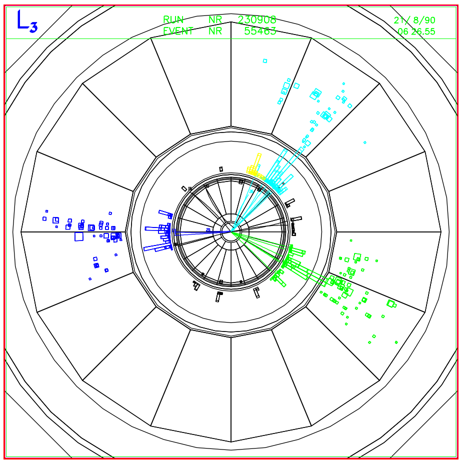

Figure 1: A three jet event detected by the L3 detector

2 The crystals and their equipment

The BGO characteristics compared to NaI are summarized in table 1. The radiation length is relatively small, and the density high, allowing for a compact detector. The light output however depends strongly on temperature.

Each crystal is 24 cm long with a front face of 2×2 cm^2 and 3×3 cm^2 for the rear face. All crystals were grown by the Bridgeman method, cut to size, and polished on all six faces at the Shangai Institute of Ceramics. They were received at CERN and tested [3] before being equipped and installed. Crystals were accepted after satisfying the following tolerances:

- Optical transmission, 55% at 400nm, 65% at 630nm
- Dimensions, 300μ in transverse, 400μ longitudinally 50μ in planarity of the faces
- Light output variations along the length, measured on a cosmic ray bench, of less than 10%

All faces are painted with a 30 to 80 μ thick coat of titanium-oxide NE560 paint for maximum light collection. The output light is read by two silicon photodiodes, Hamamatsu S-2262, of a total surface of 3.0 cm^2, and quantum efficiency Q=60%. Epoxy glue is used to fix them on the crystal. The temperature of the crystals is measured by 1792 thermal sensors placed uniformly over the whole calorimeter and situated on

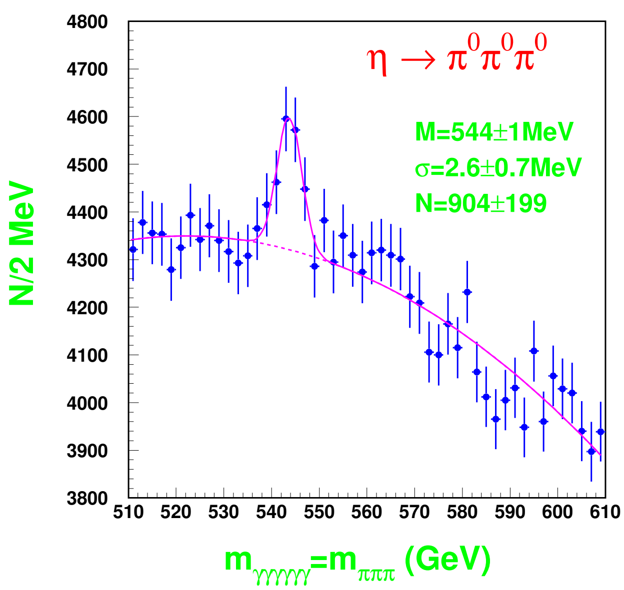

Figure 2: Invariant mass of 6 photons taken by 2

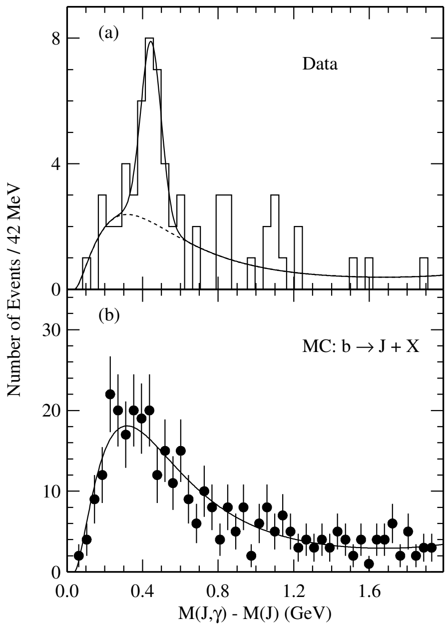

Figure 3: $\Delta M = M_{(J/\Psi)\gamma} - M_{J/\Psi}$

Characteristics	BGO	NaI
Density (g/cm^3)	7.13	3.67
Radiation length (cm)	1.12	2.59
Interaction length (cm)	22.0	41.1
Moliere radius (cm)	2.3	4.4
Wave Length (nm)	480	410
Temperature dependence ($\%/^\circ C$)	-1.55	0.22

Table 1: BGO characteristics compared to NaI

the front and rear crystal faces. Optical fibers used for light calibration are also attached to the rear face. A few centimeters away from the photodiode is a low noise charge sensitive preamplifier. It has to handle signals from a few MeV to 100 GeV, and operate in a 0.5 T magnetic field. The mean noise observed is below 1.5 MeV/channel.

3 The mechanical structure

The calorimeter consists of two half barrels and two end caps. Each half barrel contains 3840 crystals arranged in 24 θ slices and 160 ϕ slices. For the end caps the ϕ slices range from 48 to 128 across 17 radial segments making the geometry more complicated. Each crystal is placed inside an individual cell, alveoli, made of epoxy resin carbon fiber composite material. The load is transmitted to the support structure and not to neighboring crystals. There is 1 cm of carbon fiber in front of crystals, and 250μm walls between them. The total amount of material in front of the barrel crystals amounts to 0.25 radiation lengths. Figure 4 shows the mechanical structure. All θ slices are pointing to the interaction point while ϕ slices are tilted by 10mrad to avoid cracks. We observe 0.35% losses due to cracks inside the barrel.

4 Calibration with electron beams

In order to get the best energy resolution for the BGO, all the barrel crystals, and part of the end caps, were exposed to an electron beam, of 2,10, and 50 GeV at the CERN SPS, before installing the detector in L3 [4, 5, 6, 7]. Each crystal was calibrated while being situated in its final support structure, and read by the final electronics. We thus have determined the calibration constants with a high accuracy (0.6 %) which leads to the expected performance of the detector: an energy resolution better than 1.5% in a wide energy range going from 2 to 50 GeV. In addition, one half barrel was also calibrated with low energy electrons, 180 MeV from

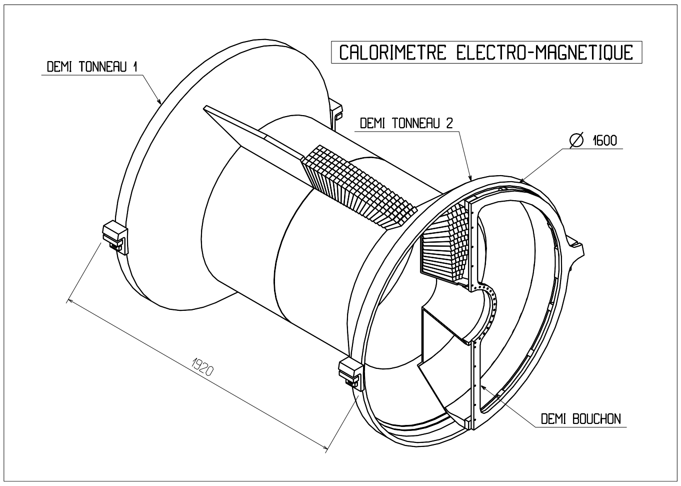

Figure 4: The mechanical structure of the BGO

the CERN LIL. Furthermore before installing the crystals inside their alveoli, we measured the uniformity and light yield with a cosmic ray bench [8]. Crystal testing, calibration and test beam efforts lasted for almost 3 years between 1986 and 1988.

4.1 Method

Given the small Moliere radius of the BGO, 93% of the energy deposited by an incident electron is spread over a crystal matrix of 3×3 around the hit crystal. Figure 5 shows the distribution of the energy measured by the central crystal (Σ_1) and the sum of 9 crystals (Σ_9) as a function of the impact point of the incident particle. Σ_9 varies very slowly, as expected. We used only events in the central region ($-7\mathrm{mm} \leq \mathrm{x}, \mathrm{y} \leq 7\mathrm{mm}$) and the Σ_9 to calibrate. An iterative method is applied, taking as initial values the cosmic ray calibration constants. After 2 or 3 iterations the variation of the calibration constant is less than 4×10^{-4}. Rear and lateral losses are taken into account by Monte Carlo as well as a small correction for the impact point. During calibration the temperature was kept constant at 18^0C.

4.2 Results

Figure 6 shows the calibration constants distribution. From the dispersion of this distribution we conclude that individual crystal calibration was necessary. The stability of the constants was checked on one half barrel which was calibrated in 1987 and 1988. The systematic error on calibration constants, includes, the uncertainty on beam momentum, the systematic error due to the

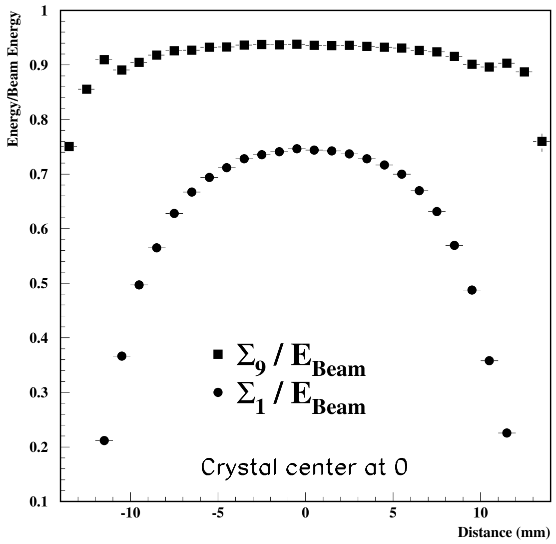

Figure 5: Energy dependence versus impact point position

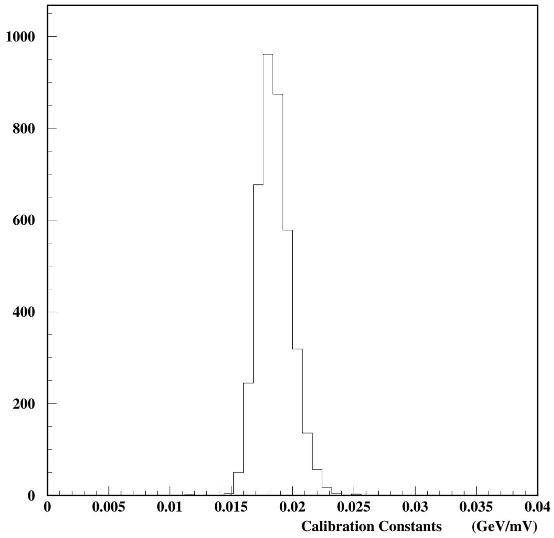

Figure 6: Distribution of the calibration constants for both half barrels

Systematic uncertainty sources	(%)
Beam momentum	0.2
Event selection	0.1
Temperature corrections	0.5
Method	0.3

Table 2: Systematic errors on calibration constant measurement

method, the uncertainty due to the event selection and finally the accuracy of the temperature correction, during this calibration run. All contributions, summarized in table 2, lead finally to a global systematic uncertainty of 0.62 %, dominated by the temperature measurement.

4.3 Energy and angular resolution

The energy of the incident particle is measured using the Σ_9, corrected for the impact point. Due to the non-Gaussian tails of the Σ_9 , the standard deviation of the distribution does not give a good estimate of its width, therefore the resolution, called local resolution, is calculated from the full width at half maximum of a functional form fitted to the distribution :

$$\begin{aligned} f &= p_1 \times e^{-p_3(x-p_2)^2} \quad if \quad x > p_4 \\ &= B \times e^{b(x-p_2)} \quad\quad if \quad x < p_4 \end{aligned} \tag{1}$$

where the free parameters are p_1, p_2, p_3 and p_4. From continuity of the function and the first derivative, we find :

$$b = -2p_3(p_4 - p_2) \qquad B = p1e^{-p_3(p_4-p_2)^2} \tag{2}$$

The half maximum of the Gaussian is at a distance $d = \sqrt{(\ln(2)/p_3)}$. If the crossover of the exponential tail is below the half maximum point the FWHM is simply that of a Gaussian. Otherwise, the width from both the Gaussian and the exponential contribute as follows:

$$\begin{aligned} FWHM &= 2 \times \sqrt{(\ln 2/p_3)} \; if \; p_4 < p_2 - d \\ &= \sqrt{(\ln 2/p_3)} + \tfrac{\ln 2}{2p_3(p_2-p_4)} + \\ & \tfrac{p_2-p_4}{2} \quad if \; p_4 > p_2 - d \end{aligned} \tag{3}$$

The resolution σ is equal to FWHM/2.35. One can see on figure 7 one typical distribution of the energy deposited in 9 crystals, for a 10 GeV incident electron, with the fit superimposed. In fact the Gaussian is a

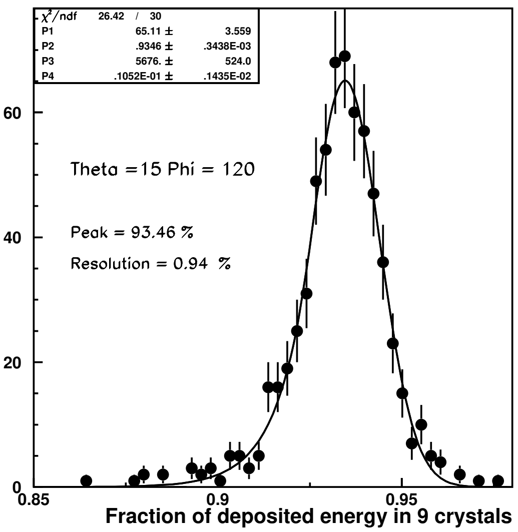

Figure 7: Local resolution and peak value for a typical crystal

good approximation for 92 % of the crystals, and the relation between the third parameter p3 and σ is simply:

$$p_3 = 0.5/\sigma^2$$

The local resolution for all available beam energies is listed in table 3. The expected local resolution is the quadratic sum of shower fluctuations, the electronic noise, and the beam momentum spread [7].

Taking into account the crystal to crystal variations we define a global resolution for each half barrel as the RMS of the mean value distribution of all crystals. In addition electronic noise has been reduced during the 180 MeV test beam. Table 4 summarizes all contributions to the overall resolution which is the quadratic sum of shower fluctuations, the electronic noise, and global resolution. We parameterize the energy resolution by the following formula, shown on figure 8 :

$$\frac{\sigma(E)}{E} = \frac{1.6 \pm 0.1}{\sqrt{(E)}} + 0.35 \pm 0.05 \quad \%$$

Impact point position is measured using the center of gravity of the shower corrected by a well known S shape function. For high energies we achieved an angular resolution of 2 mrad as shown on figure 9.

5 Calibration in situ (LEP runs)

Performing a precise calibration with electron beams is not enough for getting the best resolution during

Energy (GeV)	2	10	20	50
σ_p/p (%)	1.24	0.32	0.19	0.13
Electronic noise(%)	1.70	0.34	0.17	0.07
Shower fluctuations (%)	1.35	0.84	0.67	0.49
Expected local res. (%)	2.44	0.96	0.74	0.51
Measured local res. (%)	2.33 $\pm$ 0.06	1.00 $\pm$ 0.05	0.74$\pm$ 0.03	0.52 $\pm$ 0.02

Table 3: Local BGO resolution at different energies

Electronic noise (%)	0.35	0.09	0.05	0.02
Global res. (%)	0.42	0.30	0.27	0.24
Overall res. (%)	1.45 $\pm$ 0.06	0.89 $\pm$ 0.05	0.72 $\pm$ 0.03	0.54 $\pm$ 0.02

Table 4: Global BGO resolution at different energies

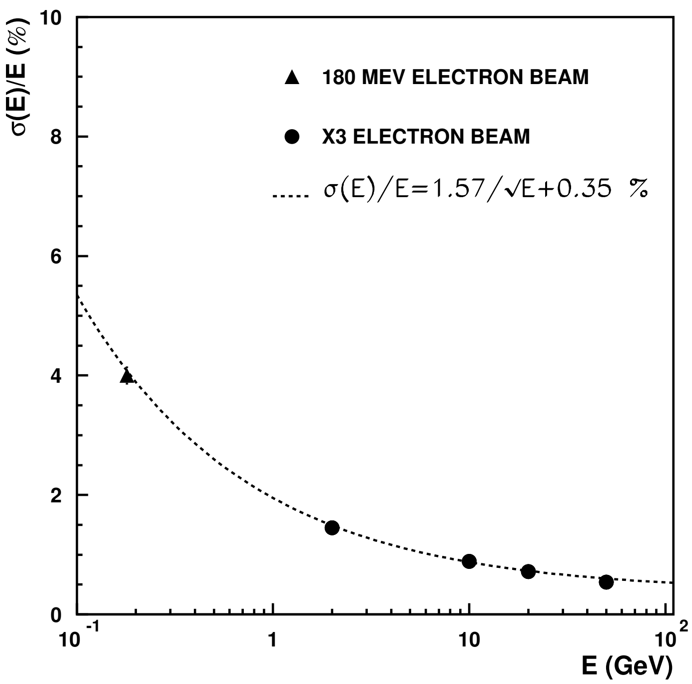

Figure 8: BGO Energy resolution : the dots represent the experimental results while the line is the fit superimposed

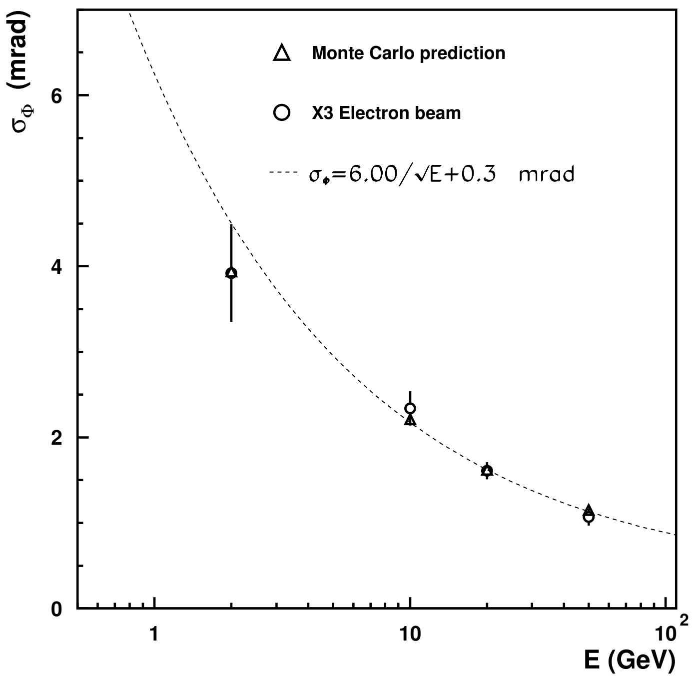

Figure 9: BGO angular resolution

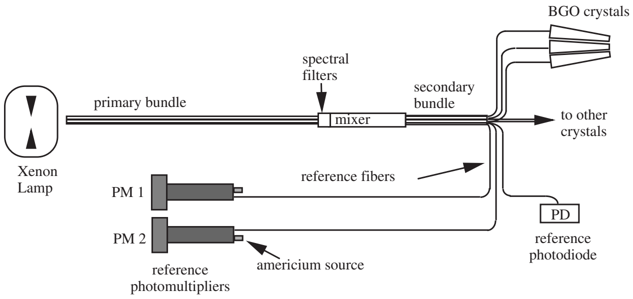

Figure 10: The Xenon system

LEP runs. One must be able to follow any light variation, due to radiation accidents for example, and any change of the electronic gains. Time dependent corrections have to be taken into account for the energy measurement. We have several ways of monitoring the light output.

- The Xenon monitor, sending light pulses
- The RFQ accelerator producing 17.6 MeV photons
- Cosmic muons
- LEP data (Bhabha events, MIP,π^0)

5.1 The Xenon monitor

A Hamamatsu L2453 Xenon lamp produces light, driven to a plexiglas mixer by 14 primary quartz optical fibers, 35m long and 600μ diameter, figure 10. Two(one) secondary optical fibers, 2 to 3m long and 200μ diameter, illuminate each barrel(end cap) crystal. The intensity for the first and second fiber is tuned to ≈ 1 and ≈ 30 GeV respectively. Crystals are grouped in geographical regions, and the calibration method consists of two steps.

- Inter-calibration. Using both fibers we adjust the calibration constants in order to get the same answer for all crystals in the same region. This value is very stable versus time, 0.2% variation over 20 days.
- The absolute scale for a region is fixed using electrons from non radiative Bhabha events.

Absolute calibration with a precision of 0.9% is achieved using the Xenon system [9] and electrons from the Bhabha process ($e^+e^- \to e^+e^-\gamma$). Figure 11 shows the normalized electron energy spectrum from end cap Bhabha events, before and after Xenon correction is applied.

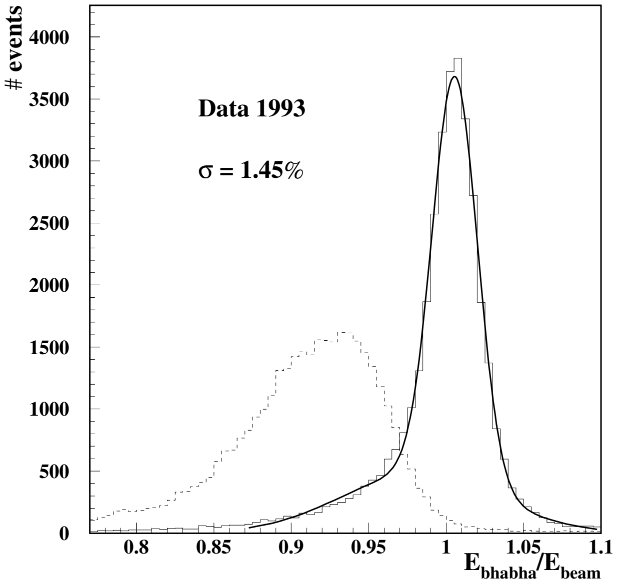

Figure 11: Electron energy before Xenon corrections (dashed line) and after.

We obtain a resolution of 1.45% for all crystals. However taking into account only the crystals for whom the Xenon calibration was possible ($\approx 93\%$) we get a resolution of 1.28%. The Xenon system is necessary to follow variations of the light collection efficiency and correct for losses.

The BGO has been running since 1989, and we observe a loss of light versus time, shown on figure 12.

We have parametrized this loss by :

$$\boxed{F(t) = \frac{a}{t+t_0} + c_\infty}$$

with

parameter	Half Barrel 1	Half Barrel 2
a(days)	233.4 ± 7.9	385.9 ± 13.0
t_0(days)	1381.6 ± 35.4	2545.0 ± 59.8
c_∞	0.830 ± 0.002	0.848 ± 0.002

For t of the order of the LEP life time we will loose 17% of the initial light. We have no explanation of this phenomenom.

Summarizing, the Xenon system is robust and reliable, necessary for the inter-calibration, but is not used

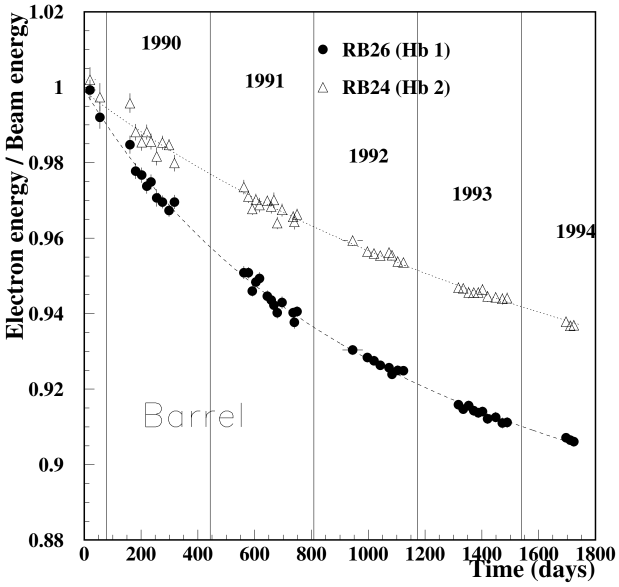

Figure 12: Light loss versus time

to give the absolute calibration, which is obtained by a physics process. However it has the ability to give an absolute measurement if needed.

5.2 The RFQ Calibration Method

A 1.85 MeV H beam from RFQ accelerator, incident on Li target provides a source of 17.6 MeV γ's via the reaction :

$$\boxed{\mathrm{p} + {}^{7}_{3}\mathrm{Li} \longrightarrow {}^{8}_{4}\mathrm{Be} + \gamma}$$

The RFQ accelerator is installed through the L3 detector and the Li target is located at the place of a missing end cap crystal. Exposure of each crystal depends on distance from target, orientation, material in front, etc. Figure 13 shows the photon spectrum on top of the pedestal contribution. The calibration constant is then defined using the edge energy $E_{\mathrm{HH+}} \sim 17$ MeV. The stability of the HH$^+$ edge determination sets the lower bound on the calibration error. An accuracy of $< 1\%$ is achieved with 900K triggers collected. Using RFQ for inter calibration in a 3×3 matrix and Bhabha events for overall energy scale we achieve a resolution for electrons of 45 GeV, of $\sigma = 1.25\%$ showing a comparable accuracy to the Xenon calibration method.

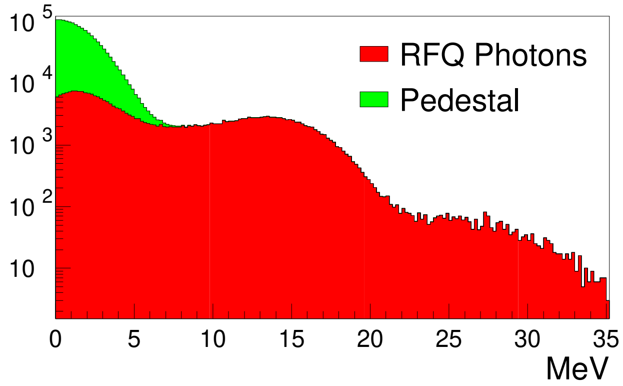

Figure 13: RFQ photon spectrum and pedestal

5.3 Cosmic muons

The energy lost by a muon that passes through a BGO crystal can be used for calibration. However this measurement is limited by errors on the track length, pedestal fluctuations, and Landau fluctuations. After only two dedicated runs, where 10^6 triggers were collected, we achieved a precision of 1.3% [10] on the calibration constants.

6 Temperature Control

Because the light output from BGO decreases by 1.55 % per $^\circ$C, it is important to have a continuous temperature measurement and monitoring. The crystal temperature is measured by two AD590 sensors glued on the front face and on the rear face of a subset of the crystals (640 for the barrel and 2×128 for the end caps). Thermal screens surrounding the BGO keep the temperature value constant and temperature gradients small. Figure 14 shows the mean temperature and its dispersion, as well as the temperature gradient between the front and rear faces. These data correspond to one year of running for the entire calorimeter. A temperature correction is applied per crystal given by :

$$\epsilon = 1 + 0.0155(\mathrm{T_c} - 18^\circ) \quad \mathrm{T_c} = \mathrm{T_f} + \eta(\mathrm{E})(\mathrm{T_b} - \mathrm{T_f})$$

Where T_f and T_b are the front and rear temperatures, and $\eta(E)$ takes into account the position of the shower maximum.

A precision of 0.2°C is achieved for this measurement.

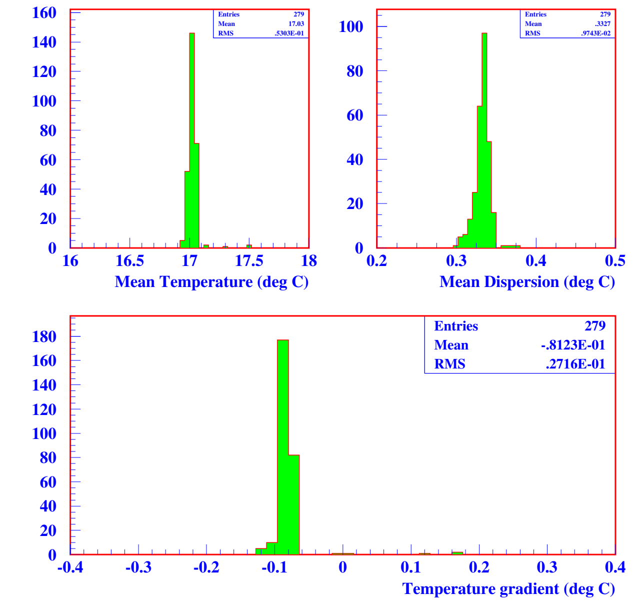

Figure 14: Mean temperature,dispersion, and gradient for 1 year of LEP running

7 Electrons and photons at LEP

Neighboring crystals with energy content higher than a threshold are grouped together to form clusters. Inside a cluster we look for local maxima, called bumps, which may correspond to an incident electron, photon, pion etc... For each bump, we define the energy, the center of gravity and an identity (electromagnetic or not).

For the energy measurement, we assume the bump to be electromagnetic, and we use the sum over the 3×3 matrix, Σ_9, around the maximum. We also correct for the rear and lateral losses, using the ratio between the energy in the central crystal Σ_1 and the Σ_9.

$$E = \frac{\mathbf{\Sigma_9}}{0.1231\frac{\mathbf{\Sigma_1}}{\mathbf{\Sigma_9}} + 0.8222} \tag{4}$$

The above correction factors used for the barrel, have been determined using 10 GeV e^- data collected at the test beam. For energies below 3 GeV, we define Σ_6 as the sum of the 6 most energetic crystal within the 3×3 matrix. A small number of crystals actively participate at low energies, therefore the use of Σ_9 or Σ_{25}, 5×5 matrix, would overestimate the incident energy due to energy contribution from the electronic noise or the nearby bumps. Σ_6 is found to consistently give the best energy estimate for low energy bumps.

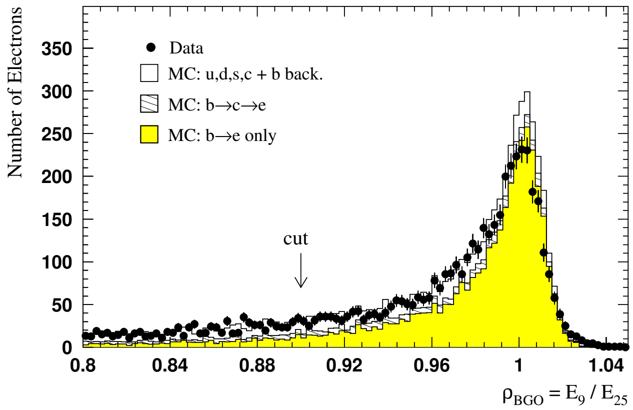

Figure 15: ρ_{BGO}, electron candidates for semi-leptonic B decays

The center of gravity g_0 is also corrected by the S shape :

$$g = \alpha \times \mathrm{Atan}(\beta g_0) + \gamma g_0 \tag{5}$$

where α, β, γ are parameters fitted from the test beam data.

Electrons and photons are identified by the energy distribution around the maximum. We mainly have two estimators :

- $\rho_{BGO} = \Sigma_9/\Sigma_{25}$. For electromagnetic particles ρ_{BGO} must be around 1.
- $$\chi^2_{BGO} = \sum_{i=1}^{9}\left(\frac{F_i - F_i^{TB}}{\sigma_i^{TB}}\right)^2 \tag{6}$$

  where F_i is the fraction of energy deposited in the crystal i (i = 1, 9), F_i^{TB} and $\sigma_i{}^{TB}$ are the fraction and the width of the fraction of energy deposited, as determined from the test beam. Normalized χ^2 must be also around 1 for electrons and photons

Figures 15 and 16 show ρ_{BGO} and χ^2_{BGO} distributions, for bumps part of events candidates for semi-leptonic B decays.

The χ^2 distribution is also used to separate single photons and merged photons from π^0 decays. More sophisticated methods are needed to reject energetic π^0 such as neural network technics. As shown on figure 17 we can reject 75% of 15 GeV π^0's, keeping the single photon efficiency very high.

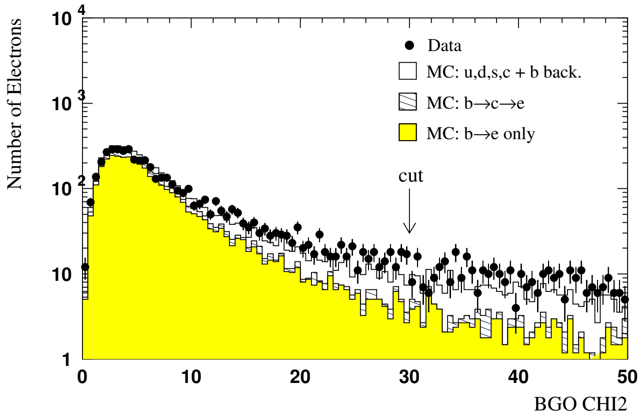

Figure 16: χ^2_{BGO}, electron candidates for semi-leptonic B decays

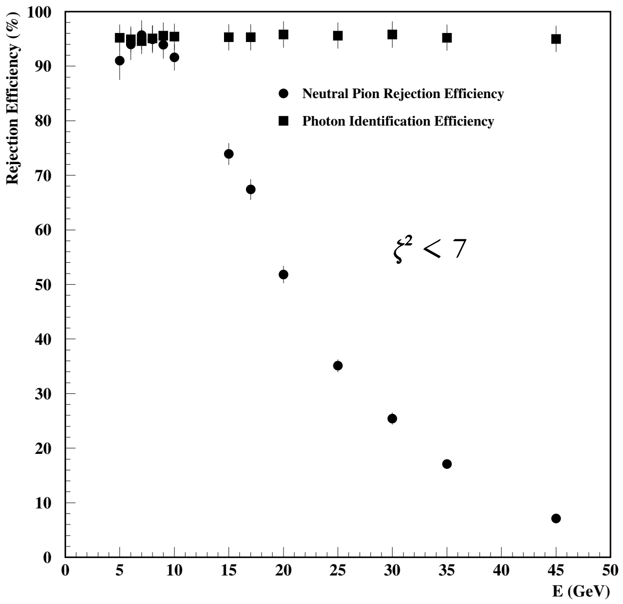

Figure 17: Single photon identification efficiency and π^0 rejection as a function of energy, with a complex algorithm.

8 Conclusions

The BGO electromagnetic calorimeter has now been running since 1989, without any particular problem. It is robust and stable detector, producing a lot of unique and first class physics. Excellent energy resolution was achieved, giving a clear advantage to the L3 detector, for all channels involving electrons and photons. If unexpected physics shows up with high statistics at LEP 100 or later at LEP 200, the L3 detector measuring with high precision all leptons and photons will be on the first line to catch it.

9 Acknowledgments

Firstly I would like to thank the organizers for inviting me to this symposium, particularly P^r He Sheng Chen. I prepared this talk with a lot of help from, D.Boutigny, D.Duchesneau, D.Kirkby, S.Rosier, C. Tully, and M.Wadhwa, who I also thank here.

References

[1] B.Adeva et al. , The construction of the L3 Experiment, Nucl. Instr. and Meth. in Physics Research A 289 (1990) 35-102

[2] O. Adriani et al., Phys. Rep. 236 (1993) 1. CERN preprint CERN-PPE/93-31; February 22, 1993.

[3] M. Schneegans, Nucl. Instr. and Meth. A257 (1987) 528

[4] C.Souyri Thesis. Calibration du calorimetre electromagnétique de L3, LAPP-T-90-03.

[5] P.E Kaaret, Thesis Princeton University (1989), DoE/ER/3072/50

[6] J.A Bakken et al., CERN-EP/89-16 , Nucl. Instr. and Meth. A280 (1989) 25.

[7] Calibration of the L3 electromagnetic calorimeter, J. Bakken et al, L3 Note 1712

[8] M. Chemarin et al, Calibration of BGO crystals with cosmic rays, CERN 88-621.

[9] A.Bay et al,NIM A321 (1992) 119-128.

[10] Results on the calibration of the L3 BGO calorimeter with cosmic rays. J.A. Bakken, et al., CERN-PPE-93-184, Oct 1993. NIM A343(1994)